Final Technical Report

Award Title: ***Estimating the Likelihood and Impact of Seismically Induced Landslides in Near Real-Time***

Award Number: **G19AP00027**

Award Term: **January 1, 2019 – December 31, 2020**

Authors:

Michael Hamburger (Dept. of Earth & Atmospheric Sciences, Indiana University, Bloomington, IN 47405; Tel: (812)855-2934 Fax: (812) 855-7899; hamburg@indiana.edu)

Anna Nowicki Jessee (Dept. of Earth Sciences, Indiana University-Purdue University Indianapolis, IN 46202; Tel: (317) 278-1475; manowick@iu.edu)

Dylan Seal and **Elizabeth Sherrill** (Dept. of Earth & Atmospheric Sciences, Indiana University, Bloomington, IN 47405)

Abstract

This report summarizes work on earthquake-triggered landslides supported by NEHRP grant no. G19AP00027, as a collaborative project between Indiana University and the USGS Geologic Hazards Science Center. The support allowed us to extend our development of a statistical model for estimating the distribution and impact of earthquake-triggered landslides in near-real time. As a direct result of this collaboration, our global model has been adapted for use in the USGS *Ground Failure* product and incorporated into the USGS's real-time reporting system. We use standardized estimates of ground shaking from the USGS *ShakeMap Atlas 2.0* to develop an empirical landslide probability model by combining shaking estimates with broadly available landslide susceptibility proxies, including topographic slope, surface geology, high-resolution land cover data, and precipitation. Our current model is based on 36 earthquakes for which digitally mapped landslide inventories and well-constrained *ShakeMaps* are available. Using logistic regression, the database is used to build a predictive model of the probability of landslide occurrence anywhere in the world, within minutes of the earthquake's occurrence. We also have developed a comprehensive dataset of the location and impact of earthquake induced landslides from 1772-2020. Using landslide fatality counts, exposure to predicted landslide probabilities and a proxy for vulnerability, we developed a model to provide order-of-magnitude estimates of the number of fatalities that could potentially occur due to earthquake-triggered landslides. Combined with near-real time *ShakeMaps*, these models can be used to make predictions of whether or not landslides are likely to occur—and if so, where—for earthquakes around the globe, along with their potential impact, as part of the USGS *Ground Failure* product. We also report on newly developed collaborations focusing on earthquake triggered landslide hazards in Costa Rica and the Central United States.

Figure 1. Example of the extensive landslides triggered by the Kaikoura earthquake. Photo by Sam Shepherd of the Royal New Zealand Defence Force.

Background

As a natural component of erosive processes, landslides present hazard in areas with large topographic relief and slope, and can result in significant loss of human life and damage to the built environment (*Daniell et al., 2017; Marano et al., 2009*). *Marano et al. (2009)* showed that 5% of fatalities related to earthquakes were caused by landsliding, and that they were the third largest contributor to fatalities, only after building collapse and tsunamis. In a recent major earthquake in Papua New Guinea, a majority of the significant impact of the earthquake was due to landslides. Earthquake-induced landslides have also been shown to be a major cause of disruption to lifelines in mountainous regions (*Bird & Bommer, 2004*), impeding emergency response efforts. Damage to transportation lifelines can result in emergency responders being unable to access to affected areas, causing delays of search and rescue efforts as well as delivery of aid. Producing timely estimates to assess the extent and distribution of hazard due to seismically induced landsliding in near real-time is thus an important aim, as this information could be used in postseismic response efforts to identify populations and lifelines likely impacted by landsliding. Estimates of the overall extent of landslide hazard can also be helpful for evaluating response strategies immediately following the occurrence of an earthquake.

Until recently there have been very few approaches that can provide real-time assessment of earthquake-induced landslides (EQIL). Our models (*Nowicki et. al, 2014*; *Nowicki Jessee et al. 2018b*) were among the first statistical models that could be readily applied globally for near real-time prediction of EQIL. Currently there are four classes of published models that could be applied globally: physical mechanistic models based on the method of Newmark displacement (e.g., *Jibson et al., 2000; Godt et al., 2008; Gallen et al., 2017*), statistical models developed with logistic regression using landslide inventories (e.g., *Nowicki et al.*, *2014*; *Parker et al., 2017*), statistical models based on fuzzy logic (e.g., *Kritikos et al., 2015; Robinson et al., 2018*), and an empirical model that relates the total area and volume of landsliding to seismologic parameters of individual earthquakes (*Marc et al., 2016).*

In this project we extend previous work on developing a globally applicable model for predicting location and human impact of landslides induced by earthquakes. Our statistical model provides a powerful new tool to predict seismically induced landslides across the globe in near-real time. Our empirical landslide probability model combines shaking estimates (from the USGS *ShakeMap* system; *Worden & Wald, 2016*) with landslide susceptibility proxies, such as topographic slope, surface geology, spatially variable ground wetness, high-resolution land cover data, and precipitation. We train the empirical model observations from a suite of 36 currently available global data sets for earthquake-triggered landslides. Its major innovation is the incorp-

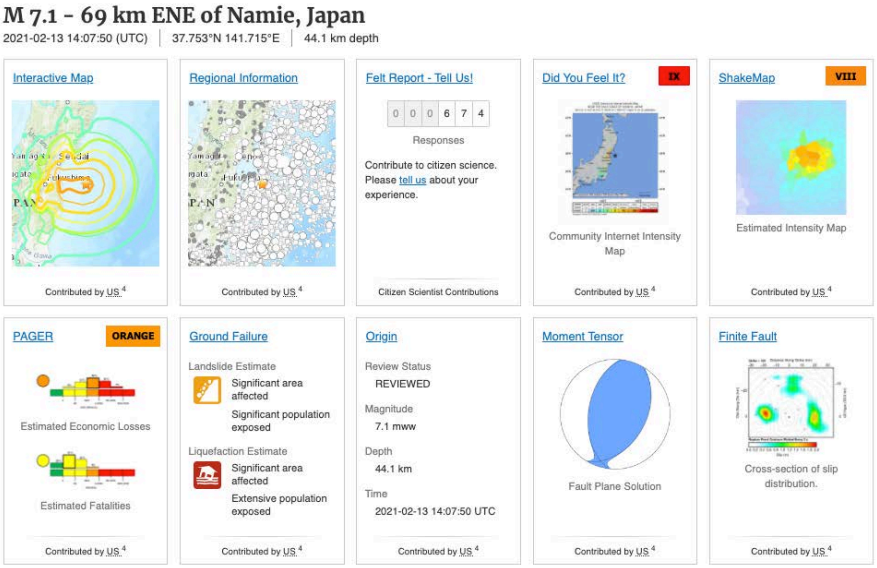

Figure 2. Example product card from the USGS earthquake monitoring system for the M7.1 Namie, Japan earthquake. Note the Ground Failure Earthquake Product indicates significant landslide hazard (orange alert) for this event.

oration of high-quality, near real-time estimates of ground shaking, together with globally available environmental data, to allow forecasting of landslide probability within minutes of the occurrence of a major earthquake. The model may be used to make predictions of whether or not (and if so, where) landslides are likely to occur for earthquakes around the globe, whether the event has already occurred or could potentially occur in the future. This approach also provides opportunities to plan for landslide occurrence in advance of damaging earthquakes, and to respond to these devastating events once they happen.

One of the most important contributions of this project is its contribution to the recently released USGS *Ground Failure Earthquake product* (*Allstadt et al., 2018b*), which makes near real-time estimates of landslide estimates for emergency response, planning, and public information, as a new "card" on the USGS earthquake information website (*earthquake.usgs.gov*), as shown in Figure 2 for the M7.1 Namie, Japan earthquake that occurred in February 2021. The *Ground Failure Earthquake Product* estimates landslide distribution and population exposure to landsliding. Our project extends the development of this model for higher-resolution landslide modeling. This will ultimately result in the development of new graphical tools to represent and assess hazard exposure to population and infrastructure (e.g., roadways, lifelines, critical facilities), comparable to a *ShakeCast* tool for ground failure.

Statistical Modeling Approach

The main objective of landslide hazard modeling is to predict areas prone to landslides either spatially or temporally *(Brenning, 2005)*; here we focus on short-term prediction of the spatial pattern of landslides triggered by an individual earthquake. Our methodology, summarized in Figure 3, uses a statistical approach, following those applied in many previous landslide studies, including *Jibson (2007)*, *Garcia-Rodriguez et al. (2008)*, *Felicísimo et al. (2012)*, and *Li et al. (2012)*. Landslide hazard assessments typically involve creation of a long-term landslide susceptibility map as their end product and are usually focused on a small region where data are available at a relatively fine resolution. Our approach takes this statistical method to a global scale, making use of high-quality, near real-time ground shaking estimates from *ShakeMap*, along with globally available susceptibility proxies, to estimate landslide probability within minutes after a major earthquake.

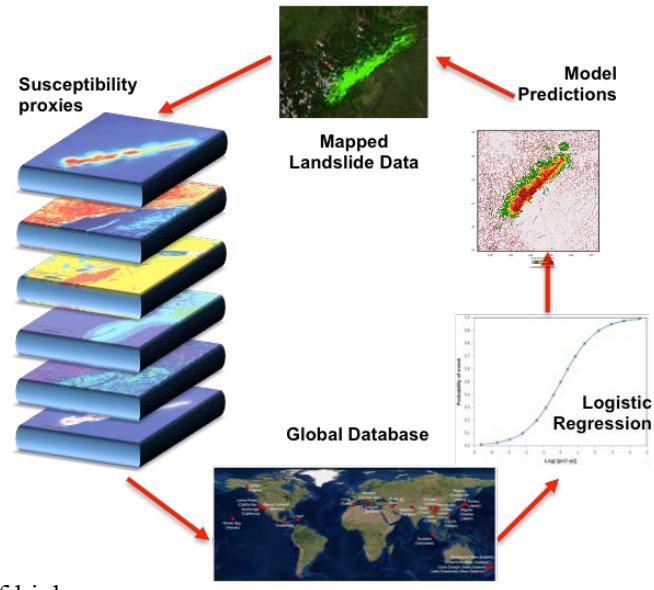

Figure 3. Schematic showing model development.

We apply logistic regression analysis (e.g., *Peng et al., 2002*) to a series of training events with well constrained ground shaking and landslide distribution data, which provide empirical constraints on the model. The performance of the regression model is assessed with both statistical goodness-of-fit metrics and a qualitative review of the model's capability to capture the spatial extent of landslides for each training event, as well as for validation test events that are not used in the regression model. Combined with near real-time *ShakeMaps*, the model may be used to make generalized predictions of whether or not (and if so, where) landslides are likely to occur for earthquakes around the globe.

We use logistic regression (e.g., *Rennie, 2003*) to represent a process involving a binary outcome (in this case, *slide* or *no slide*), which allows us to fit the observed outcomes to the logistic function using data representing multiple predictor variables. The logistic function transforms the odds of an outcome into a probability value, as shown in Equation 1. Following *Brenning (2005*) we conclude that logistic regression provides the most reliable statistical approach for modeling seismically induced landslides.

$$Logit(P) = \ln\left(\frac{P}{1-P}\right) = a + bx_1 + cx_2 + dx_3 + \cdots \quad (1)$$

The probability of an outcome can then be represented by Equation 2:

$$P(t) = \frac{1}{1+e^{-t}}, \quad (2)$$

where $t = a + bx_1 + cx_2 + dx_3 + \cdots$

and $x_1, x_2, x_3, \ldots$ represent the explanatory variables; and *a*, *b*, *c*, and *d* are coefficients determined in the regression.

While landslide susceptibility maps are currently available for various regions, as well as some available globally (e.g., *Nadim et al., 2006*), none allow for real-time input into their model, as they represent a long-term susceptibility to landslides. Our goal is to incorporate the hazard estimate from seismic events by including the *ShakeMap* data for each earthquake (available in near real-time from the USGS), combined with both slope values and proxies for material strength, wetness, and soil strength, thus allowing the model to be applied in near real-time for future events.

Our modeling assesses quantitative relationships within the data, using logistic regression to establish a functional form between the predictor variables and the outcomes (Figure 3). Metrics of success to test the model performance include visual interpretation (spatial correlation), the Akaike Information Criterion (AIC; *Wagenmakers & Farrell, 2004*), the area under the receiver operating curve (AUROC; *Marzban, 2004*), graphical performance classifications, and qualitative assessment of the models in terms of their predictions in parameter space.

While the method of logistic regression has been widely used, its global application has been limited by a number of characteristics. First, most of the applications in the literature are developed within local projects, e.g., within one country—and thus are seldom applicable outside that study area. Second, the input parameters representing the shaking hazard vary from project to project, thus making it difficult to compare results from similar landslide susceptibility studies. Finally, in many cases no method is provided to test how well the model is performing. This project addresses these large gaps in the literature in order to present a *globally applicable, short-term, probabilistic estimate of the likelihood of landslides associated with a particular event*.

Predictor Variables

We examine a range of physical properties and hydrologic conditions of near-surface materials and the characteristics of ground shaking during an earthquake that may affect the location, size, and mobility of earthquake-triggered landslides. We rely on empirical studies that describe known impacts on the distribution of landsliding to choose globally available predictor variables that can represent the susceptibility of an area to landsliding—combined with triggering ground motion estimates from *ShakeMap*. Based on these guidelines, we initially include the following predictor variables in the regression analysis for further testing: (1) ground motions produced by the earth-

quake, (2) topographic slope, (3) elevation, (4) lithology, (5) soil wetness, (6) precipitation, (7) land cover, and (8) earthquake magnitude. These variables were quantitatively compared with the spatial distribution of mapped landslides that occurred due to shaking produced in that particular event.

Landslide Data. The element most critical to our proposed work is a growing data set of observational landslide data from 36 earthquake-triggered landslide events. The current locations of sources are shown in Figure 5. Multiple methods are used to map landslides; these include field-based mapping of observed landslide deposits and remote sensing techniques. These 'training events' have been selected based on the quality and availability of data for these events. Figure 4 shows a comparison of the predicted landslide probabilities and the mapped landslides caused by the 1999 Chi-Chi, Taiwan earthquake. As an outgrowth of this project, we have collaborated with landslide researchers from USGS and University of Twente (Netherlands) to publish the landslide inventories from this global suite of events in an open-source global database, as described in *Tanyas et al.* (*2017*) and *Schmitt et al. (2017)*, which will open the door to provide open access data for further studies within the landslide community.

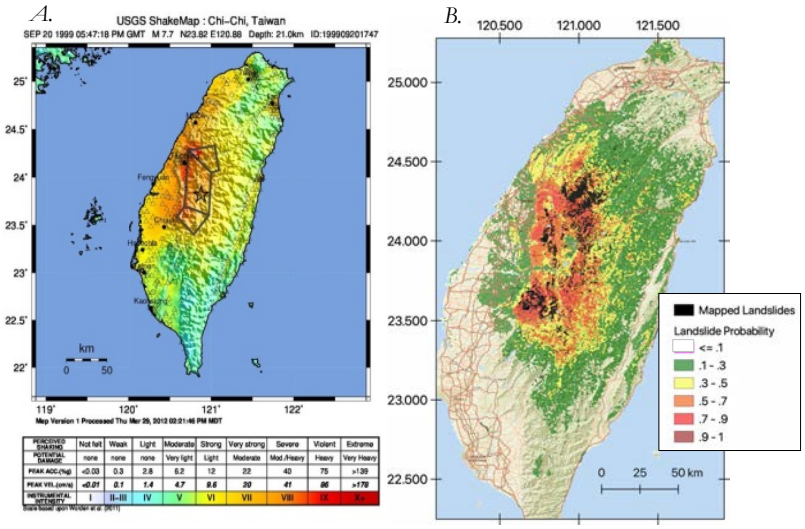

Figure 4. (a) ShakeMap output showing MMI (Modified Mercalli Intensity) for the September 20, 1999 Chi-Chi, Taiwan earthquake (Garcia et al., 2012). (b) Spatial distribution of mapped landslides due to the earthquake, shown with black dots (Liao and Lee, 2000) overtop of predicted landslide probabilities from the Jessee et al. (2018) landslide model.

Ground motion. Many studies have shown that landslide patterns reflect properties of the triggering ground shaking (e.g., *Verdin, 2017; Keefer, 2002; Meunier et al., 2007; Nowicki et al., 2014; Rodriguez et al., 1999)*. Here we test a number of estimates of ground motion parameters available from the USGS *ShakeMap* system (*Worden & Wald, 2016)* including peak ground acceleration (PGA), peak ground velocity (PGV), and Modified Mercalli Intensity (MMI). We note, however, that the *ShakeMap* estimates of ground motion amplitudes evolve in the hours and days following an earthquake as new source models and strong-motion and intensity data become available. As a result the resulting landslide probabilities change significantly, as shown by *Allstadt et al. (2018a,b)*.

Topographic Slope. Slope steepness exerts a strong control on slope stability (e.g., *Budimir et al., 2015*). We attempt to incorporate slopes computed from the highest resolution elevation data that are consistently available globally. We incorporate a new, globally available slope dataset at 3 arc second (~90 m) resolution, published in *Verdin* (2017) in this round of model development.

Lithology. We use a newly available global lithological map (GLiM) dataset available for the entire globe *(Hartmann & Moosdorf, 2012)*. This dataset provides the most detailed representation of lithology tested here by combining 92 regional lithological maps at the highest resolution available from across the globe. We use their 13 classes of lithology and also classify the lithologies into relative strengths based on the ranking system of *Nadim et al. (2006)*. We recognize that soil cover is highly variable and plays a role in near-surface landsliding, which is not accurately reflected in the GLiM data. We therefore also test a soil thickness dataset at 250-meter resolution from the Soil Grids data, a soil depth dataset, and a soil taxonomy dataset.

Material Wetness. In order to incorporate variability in surface wetness into the landslide model we use the compound topographic index (*CTI*) as a proxy for potential soil wetness *(Moore et al., 1991)*. We also test a 3 arc-second resolution dataset of CTI published in *Verdin* (2017). CTI combines the slope value (a) and the contributing basin area (A) to estimate the spatial variability of wetness within a landscape,

$$CTI = \ln\left(\frac{A}{\tan(\alpha)}\right). \quad (3)$$

High CTI values thus result from lower slope values with larger drainage areas, while low CTI values result from higher slope values with smaller drainage areas. We recognize that this value does not consider soil moisture directly but is dependent on the potential influence of topography on soil wetness (i.e., drainage area and proximity to a stream).

Land Cover. Vegetation type and coverage can affect the composite strength of the soil-vegetation root matrix, which affects the stability of a slope. The overall effect on strength can be variable and highly dependent on localized properties. We therefore use land cover data in our model as a proxy for vegetation cover by including the GlobCover 2009 data, available at 300 m resolution, based on satellite imagery from multiple sources during 2009 *(Arino et al., 2012)* and separated into 20 classes. We also tested a percent green vegetation cover dataset derived from MODIS data.

Project Results

Since this collaborative project was initiated in 2012, we have made considerable progress in developing a workable model for near real-time landslide prediction. Our results, presented by *Nowicki et al. (2014)* and *Nowicki Jessee et al. (2018; 2019),* used a number of well-documented case histories in the landslide literature to build the database of landslide observations that are used as a training set for our predictive model. These events were selected based on the high quality and availability of data. As part of this effort, we have helped to develop an open repository of landslide inventories described in *Tanyas et al. (2017)* and *Schmitt et al. (2017)*. Our current landslide model includes 36 events from various regions, as shown in Figure 5 (from *Nowicki Jessee et al., 2020b*). Data for additional earthquakes will be incorporated as new, high-quality landslide data become available.

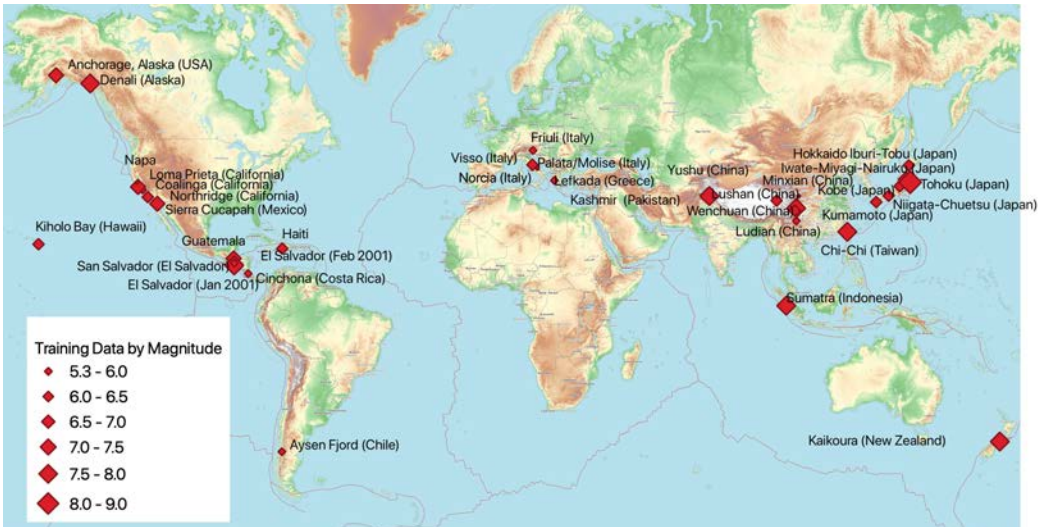

Figure 5. Map of events incorporated into training the global database.

Modeling with increased resolution. Until recently, our modeling was limited to 7.5 arc-second (~250 meter) resolution. Because the majority of landslides—and their associated impacts—are controlled by topographic irregularities at scales significantly smaller than this, we increased the spatial resolution of our model through application of a newly available higher resolution topography dataset *(Verdin, 2017)*, which provides slope data at 3 arc-second (~90m) resolution south of 60 degrees N and 7.5 arc second (~250m) resolution north of 60 degrees N. Results show this may allow us to more accurately model landslide occurrence. A comparison between the slope data developed at 30 arc-second, 7.5 arc-second, and 3 arc-second resolutions is shown in Figure 6. Note the higher variability and detail present in the 3 arc-second data.

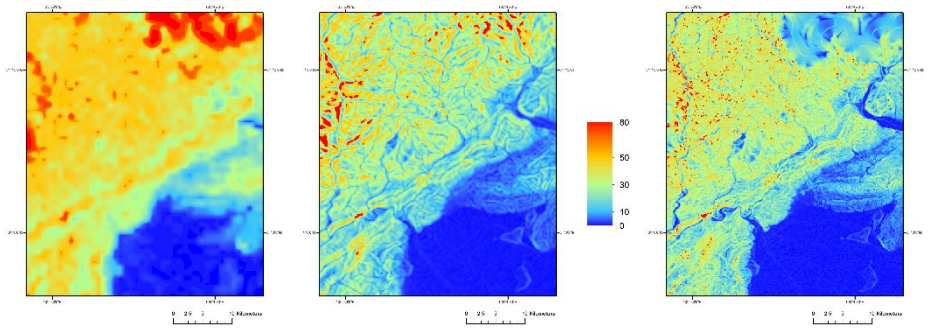

Figure 6. Comparison of slope data calculated for the 2008 Wenchuan earthquake region at 30 arc-second resolution (left), 7.5 arc-second resolution (middle) and at 3 arc-second resolution (right).

Improved/new input parameters. We also tested newly available, updated global data sets for incorporation into the landslide model. These include the datasets given in Table 1. A comparison between previously tested data and newly tested input parameters chosen to be used in versions of the model moving forward is shown in Figure 7.

Table 1. Newly tested landslide susceptibility proxies available globally.

Global Data Layer Description	**Source**	**Resolution**
Maximum Temperature of Warmest Month (BIO5)	Fick and Hijmans, 2017. Worldclim 2: New 1-km spatial resolution climate surfaces for global land areas. International Journal of Climatology. https://www.worldclim.org/data/bioclim.html	1km
Mean Annual Precipitation (BIO12)	Fick and Hijmans, 2017.	1km
Precipitation Seasonality (coefficient of variation; BIO15)	Fick and Hijmans, 2017.	1km
MODIS % Green Vegetation Cover	Broxton et al. 2014b, A MODIS-Based 1 km Maximum Green Vegetation Fraction Dataset, J. Appl. Meteorol. Clim.	1km
Soil Thickness	SoilGrids250m, Absolute depth to bedrock (in cm), http://soilgrids.org BDTICM_M_250m_ll.tif	250m
Soil Taxonomy	SoilGrids250m, Predicted WRB 2006 subgroup classes (as integers), http://soilgrids.org TAXNWRB_250m_ll.tif	250m
Average Sediment Depth	Pelletier et al. 2016. Global 1-km Gridded Thickness of Soil, Regolith, and Sedimentary Deposit Layers	1km
3 arc-second Slope	Verdin, K.L., 2017, Hydrologic Derivatives for Modeling and Applications (HDMA) database: U.S. Geological Survey data release, https://doi.org/10.5066/F7S180ZP.	~90m south of 60°N and ~250 meter resolution north of 60°N
3 arc-second Compound Topographic Index (CTI)	Verdin, K.L., 2017, Hydrologic Derivatives for Modeling and Applications (HDMA) database: U.S. Geological Survey data release, https://doi.org/10.5066/F7S180ZP.	~90m south of 60°N and ~250 meter resolution north of 60°N
Vs30	USGS (*Worden & Wald, 2016)*	1km

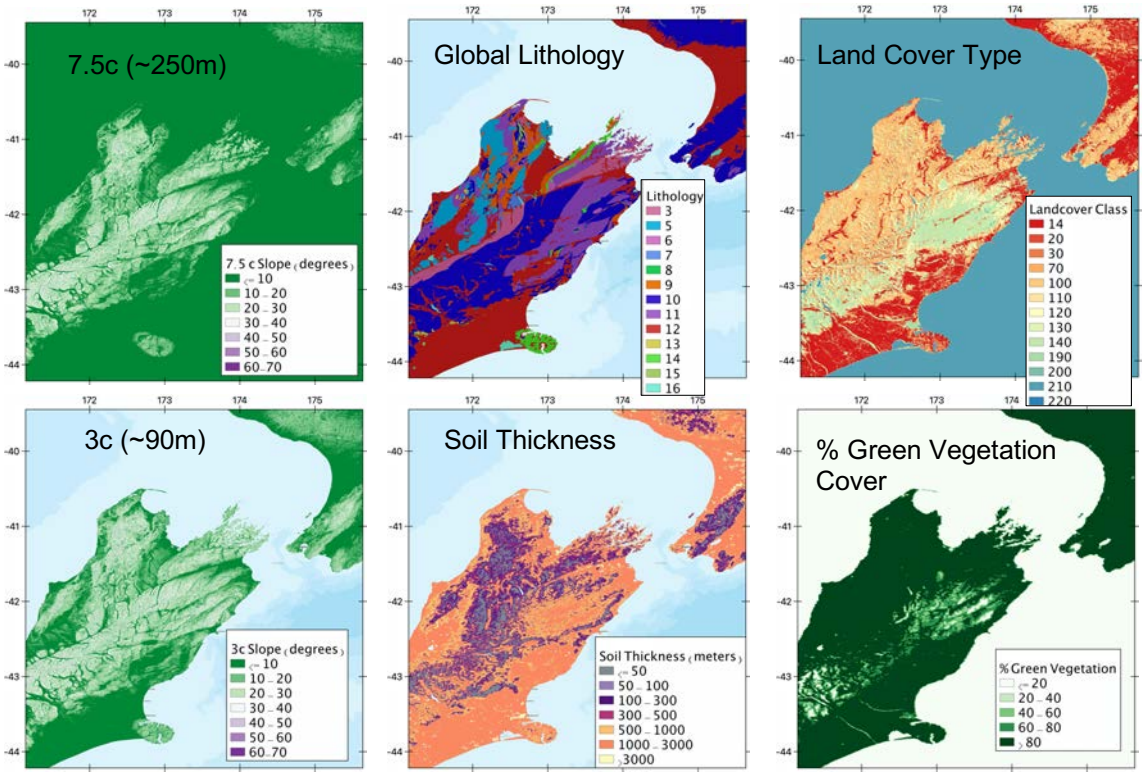

Figure 7. Comparison of newly tested landslide susceptibility proxies and previously tested data in the region surrounding the Kaikoura earthquake in New Zealand (2016). Left column shows slope data calculated at 7.5 arc-second resolution (top), and 3 arc-second resolution (bottom). Middle column shows GIIM lithology (top) and soil thickness (bottom). Right column shows land cover type (top) and percent green vegetation cover (bottom).

Model Testing and Selection

We iterate over numerous combinations of predictor variables to find the best-fit model of all the combinations that can be used in the regression. We compare the AIC and AUROC values as a metric of model performance; due to its prominence in the literature and ability to differentiate model combinations from one another, we choose the AUROC as our principal measure of model fit, where the highest value indicates the best fit of the model to the data. However, we see that high AUROC values also result in low AIC values for a given model configuration, which represents the best model fit, and therefore we can use the two measures in conjunction to determine a best-fit model.

Preliminary testing used proxies for shaking, slope, lithology, wetness, mean monthly precipitation, land cover, and magnitude, yielding a best-fit combination that results in the lowest AIC value of all variable combinations. At a finer scale, we then introduce various representations of each variable (where available), while holding all other model parameters fixed. Results then show which variable portrayal results in a better fitting model. Model testing shows incorporating 90m slope data produces a model that fits about as well as the 250m slope data we are currently using, but not better. These test results also show that models produced with other slope stability measures such as soil thickness and percent green vegetation cover fit the landslide data nearly equally as well as more complex datasets of lithology and landcover.

We present three different model formulas to allow downstream users of the model to choose which model formula will work best for their application of the model. Using this method, we find three best-fit models, starting with a functional model form shown in Equations 4 and 5 (from *Nowicki Jessee et al. 2018)*:

$$z = a + b*ln(PGV) + c*(Median\ slope) + d*(Lithology) + e*(Land\ Cover) + f*(PGV*Slope) + g*(CTI), \quad (4)$$

where ***a***, ***b***, ***c***, ***d***, ***e***, ***f,*** and ***g*** are coefficients solved for in the regression, and

$$P(z) = \frac{1}{1+e^{-z}}, \quad (5)$$

where *P* = predicted probability of landslide occurrence.

The models and their associated goodness-of-fit estimates are summarized in Table 2. Model 13 adds an additional variable of soil thickness data. Model 14 uses the higher resolution 3 arc-second slope and CTI data and adds an additional variable of soil thickness data. In Model 17 we replace the nominal variables previously used in the model with numerical values. Soil thickness data replaces lithology categories, and percent green vegetation cover data replaces land cover categories. The goal of this final model is to eliminate some of the problems that have been found when using these two nominal datasets in near-real time as part of the *USGS Ground Failure* Tool.

Table 2. Comparison of three favored models for landslide occurrence. From Nowicki Jessee et al. (2020b).

Model	Model # 13 (high-res topo + soil thickness)	Model # 14 (250m topo + soil thickness)	Model # 17 (250m topo + numerical geology/land cover)
AUC Value	0.917	0.923	0.901
AIC Value	448652	436815	497789

The 36 landslide data sets described above were used to calibrate these models, and results were presented by *Nowicki Jessee et al. (2020b)*. The coefficients solved for from this 'global' dataset are then termed the 'global landslide models,' and can be applied to each event in a forward sense in order to determine how the model performs in each location. Spatial predictions from these global models as applied to the M7.7 Chi-Chi, Taiwan earthquake are shown in Figure 8, where each of the plots shows the spatial pattern of the model output predictions in comparison to mapped landslides triggered by the earthquake. All three newly developed models provide a good fit between predicted landslide probabilities and the landslide inventory for the Chi-Chi, Taiwan case study. By zooming in to smaller areas of the map (Figure 9) we can observe differences in the results out of the three models as compared to the current published version of the model. These visual results suggest that Model 13 (3 arc-second slope and CTI data + soil thickness) reduces over-prediction of landslide probability and can recreate detailed features of landslide occurrence better than the other models.

These results yield three new preliminary models for global application to predict landslides associated with future large earthquakes. To apply these models for rapid response and loss estimates (post-earthquake occurrence), the inputs for the forward model are simply the location of the earthquake, and the spatial distribution of peak ground velocity, which is computed via the *ShakeMap* program.

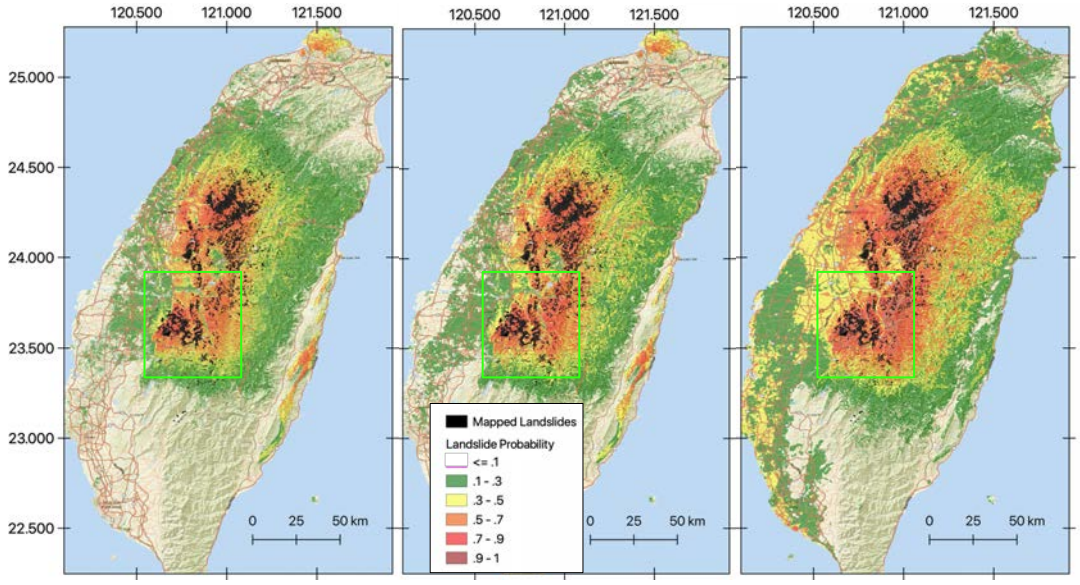

Figure 8. Predicted landslide probabilities for the area surrounding the M_w7.7 September 20, 1999 Chi-Chi, Taiwan earthquake out of Model 13 (3 arc-second resolution + soil thickness added; left), Model 14 (7.5 arc-second resolution + soil thickness added; middle), and Model 17 (7.5 arc-second resolution with numerical geology and landcover data; right). Black dots indicate landslides used for training the model (Liao and Lee, 2000).

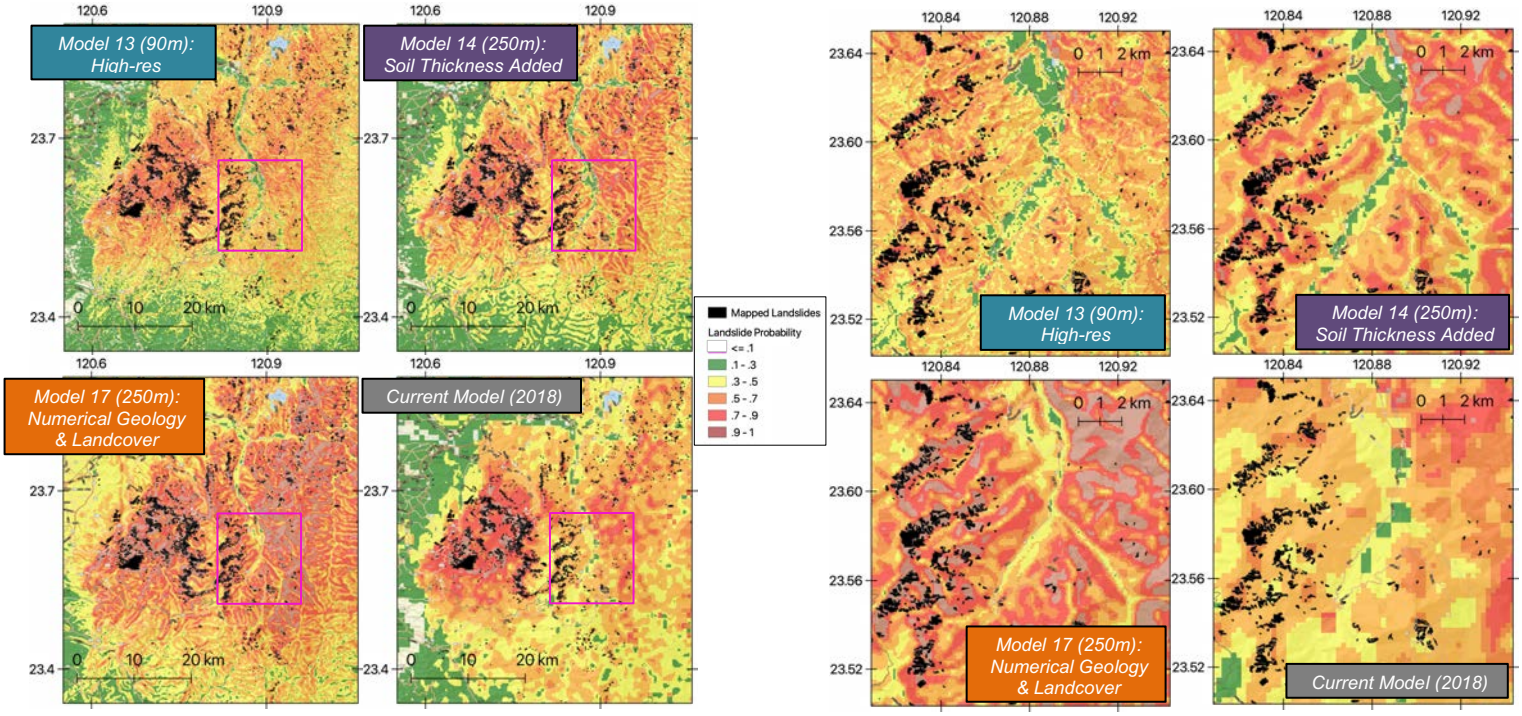

Figure 9. Landslide probability estimates out of four versions of the landslide model for the M_w7.7 Chi-Chi, Taiwan earthquake that occurred on 9/20/99. Left panels show an inset of Figure 5, while the right panels show a further inset (as indicated by the area within the pink box on the left panels). Black dots indicate landslides used for training the model (Liao and Lee, 2000).

Analysis of EQIL impacts – fatality estimation

Currently, there are many datasets describing landslides caused by individual earthquakes, and global inventories of earthquake-induced landslides (EQIL). However, until recently, there were no datasets that provide a comprehensive description of the impacts of earthquake-induced landslide events. In our *ScienceBase* data release (*Seal et al., 2020*), we present an up-to-date, comprehensive global database containing all literature-documented earthquake-induced landslide events for the 244-year period from 1772 through May 2020. The database represents an update of the catalog developed by *Nowicki Jessee et al. (2020a)*, which summarized events through 2016. The revised catalog contains 264 historical earthquakes, 153 of which include documented landslide fatality counts. The global distribution of coseismic landslide fatalities is shown in Figure 10. Our dataset includes information on earthquake size, depth, earthquake fault type, date and time, location, the availability of a USGS *ShakeMap*, availability of a landslide inventory, information about landslide occurrence (number of landslides, area or volume of landsliding, landslide magnitude), and earthquake/landslide impact (total fatalities, landslide fatalities, and number of injuries due to the effects of the earthquake). Users may download both the database of all known EQIL events, and all events for which landslide fatality counts exist, on the *ScienceBase* website.

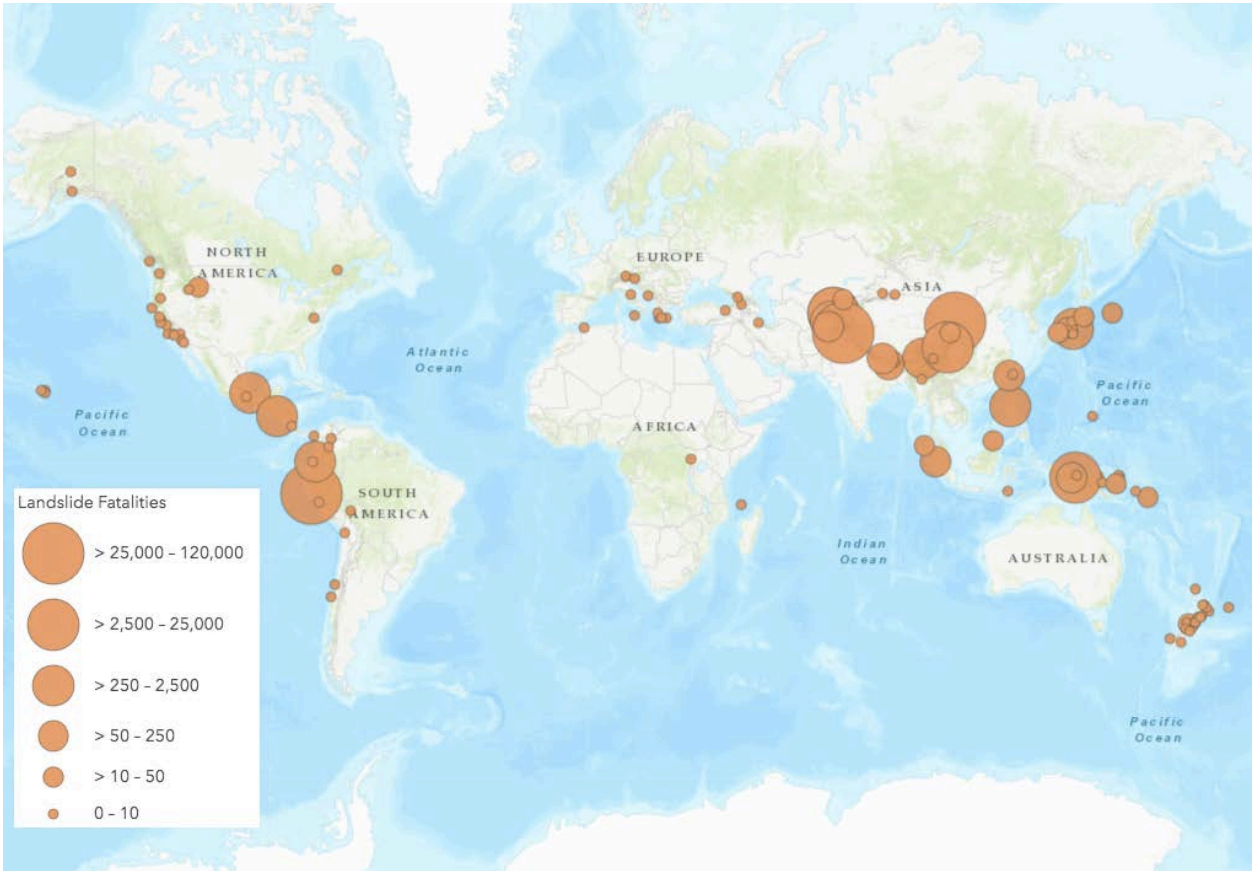

Figure 10: Global map of all documented earthquake-induced landslide events occurring between 1772 - May 2020 that contain recorded landslide fatality counts. Events are scaled by the quantity of landslide fatalities per event, represented by varying circle sizes on the map.

In order to develop a quantitative model of impact due to earthquake-induced landslides, we used this global dataset to develop a predictive model of landslide fatalities trained using 91 of these earthquakes with landslide-related fatality observations for which *ShakeMaps* are available. Our best-fit model is a multiple linear regression between probabilistic landslide exposure (PLEI), the *United Nations Human Development Index* (UNHDI; as a proxy for vulnerability), and fatality count from past earthquake-induced landslide events. There is a positive correlation between $\log_{10}$(PLEI) and $\log_{10}$ (observed fatalities) (r=.507, p<.001), as well as a high negative correlation between UNHDI and $\log_{10}$(observed fatalities) (r= -.491, p<.001). The regression yields the model shown in Equation 6:

$$log_{10}(P_{fatality}) = 0.639 + 0.417 * log_{10}(PLEI) - 2.939 * (UNHDI) \quad (6)$$

We apply this model to all of the training data; the results are shown in Figure 11. We find that the fatality predictions generally fit the data well, with significant exceptions for three anomalously large fatality observations (the Peru earthquake of 1970, the Kashmir, Pakistan earthquake of 2005, and the Wenchuan, China earthquake of 2008), as shown by the difference between the observed and predicted landslide fatality counts for each of the earthquakes in Figure 11. In general, we observe an inverse relation between the fatality rate per exposure to landsliding and the human development index values, suggesting higher vulnerability among countries with lower UNHDI values. We observe a significant positive correlation between predicted and observed fatalities, but with high variability in fatality rates for similar exposure levels.

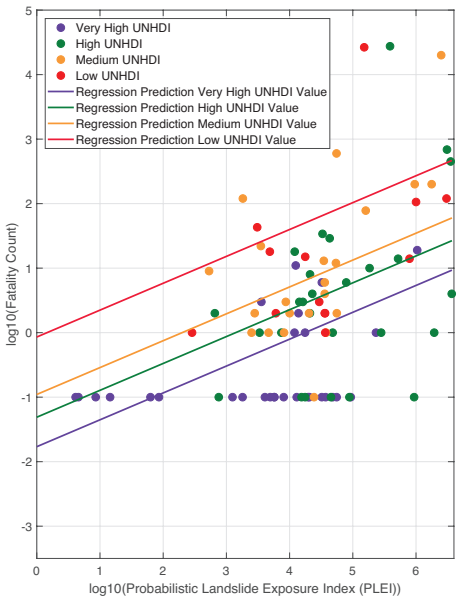

Figure 11. Multiple regression on $\log_{10}$(landslide fatalities) dependent on $\log_{10}$(PLEI) and UNHDI. Each line represents the model prediction calculated using the mean value of the four classes of UNHDI defined by the United Nations Development Programme (UNDP, 2016).

These estimates of potential landslide fatalities can also be used together with scenario earthquakes described here to understand the potential for landsliding in an area prior to the occurrence of a large earthquake. Together, these products provide a basis for a more comprehensive understanding of potential landslide impacts, whether estimated prior to or after a large earthquake occurs. The results can be used by vulnerable communities to improve land-use planning, structural design, and emergency response in landslide-prone areas.

Incorporation into USGS Ground Failure System

The current version of our published landslide model is being used by the USGS *Ground Failure Earthquake Product* to estimate landslide hazard in near-real time after large earthquakes around the world, for which *ShakeMaps* are produced. These estimates are also being used for estimating population exposure to landslide estimates. This tool has undergone the final beta testing phase and is now available publicly (*Allstadt et al., 2018b).* Figure 12 shows an example of the ground failure product as applied to the M7.1 Namie, Japan earthquake of February 2021. This event was shown to have significant landslide hazard as well as significant population exposure, which is depicted on the hazard estimates from the *Ground Failure Earthquake Product.*

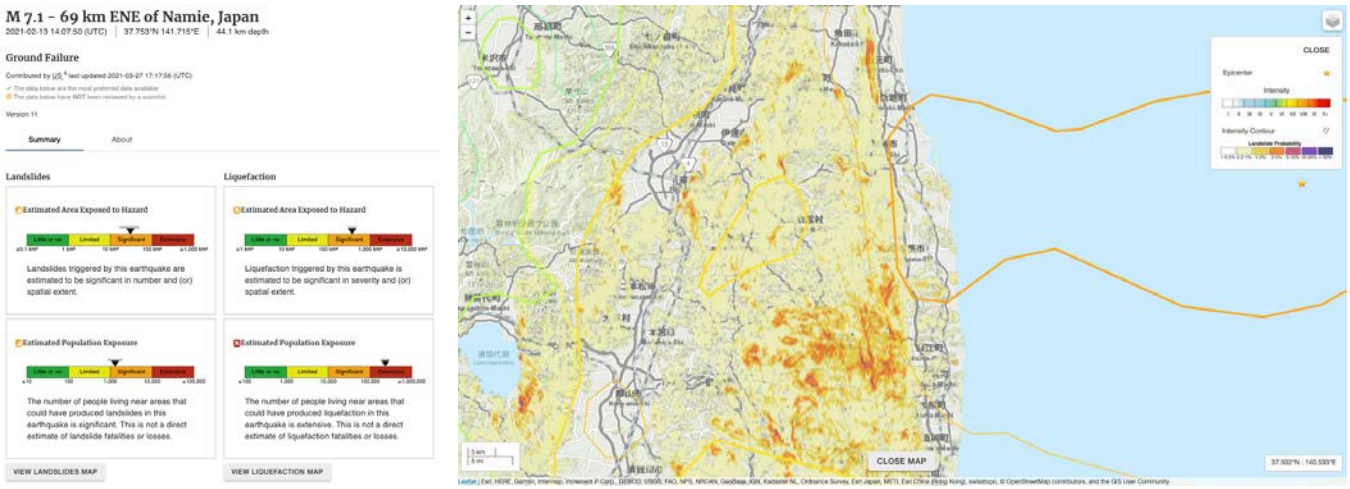

Figure 12. An example of the USGS Ground Failure Earthquake Product output for the Namie, Japan earthquake that occurred on 02/13/21. Note the two separate alert levels for landslide hazard and landslide exposure (left), as well as the map of estimated landslide distribution (right). These products are available in near-real time for every significant earthquake (M_w6.0 and larger) around the world for which a ShakeMap is produced.

Contribution of Fatality Estimation in the Ground Failure product

We plan to continue our current collaboration with the USGS to continue developing and testing the landslide models for further development with the USGS *Ground Failure Earthquake Product*. In particular we will work together with USGS colleagues to tie alert levels to estimated fatality bounds out of the fatality model (after further development described in the previous section), to produce a product similar to the *PAGER* outcome for earthquake fatalities. A preliminary alert level designation is shown in Figure 13.

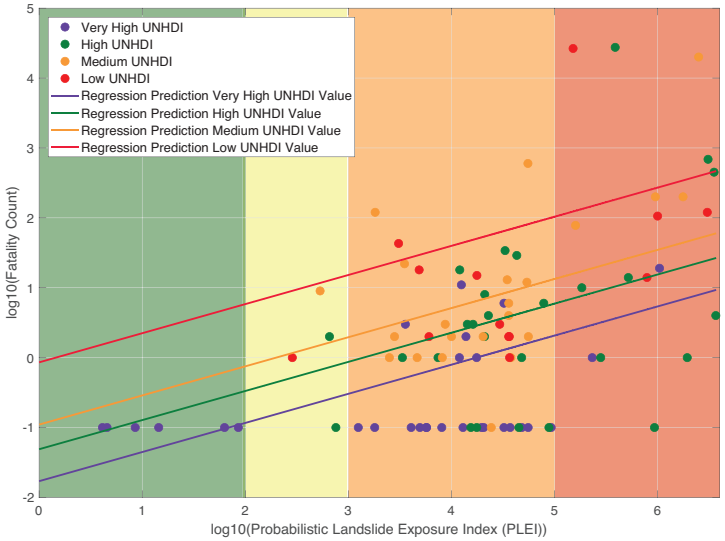

Figure 13. Observed earthquakes (dots) plotted in terms of exposure and fatality count. Multiple regression model is plotted on top. Shading indicates an initial proposed alert level designation.

Deterministic landslide predictions with scenario earthquakes

The USGS *ShakeMap* system permits, in addition to rapid prediction of strong ground motion in the aftermath of earthquakes, the analysis of 'artificial' earthquakes, as a contribution to deterministic earthquake hazard assessment (e.g., *Hamburger et al.,* 2011). The same approach can provide a powerful tool to assess spatial patterns of future landslide hazards in areas of known landslide vulnerability. The USGS has developed an archive of 'scenario earthquakes' that allow forecasting of expected ground motion and potential impacts of specific hypothetical large earthquakes that can be used for planning emergency response and hazard mitigation. Given that the landslide regression model is framed by *ShakeMap* estimates of ground motion, the system could be readily adapted to provide estimates of potential landslide vulnerability, as shown in Figure 14 for scenario earthquakes in Northern California, the Pacific Northwest, and the central U.S. By utilizing the global landslide

model to predict where landslides are to occur due to a particular scenario earthquake, we can identify areas that are more and less prone to earthquake-triggered landslides.

Estimates of landslide impacts, in collaboration with use of these scenario earthquakes, will provide a powerful tool for communities to understand and respond to the risk associated with earthquake-induced landslides. Estimates of potential landslide fatalities can also be used together with scenario earthquakes described here to understand, and ideally, prepare for, the potential impact of landsliding in an area prior to the occurrence of a large earthquake. These estimates can be used by vulnerable communities to improve land-use planning, structural design, and emergency response in landslide-prone areas. By understanding their proximity to this type of hazard before the occurrence of a destructive earthquake, our work may ultimately contribute to improved community resilience to both natural and human-induced disasters. We have applied this to different case study areas in Costa Rica and the Central U.S. to investigate the impact of source location, depth, source faulting, and magnitude on landslide occurrence to provide a more robust understanding of potential for landsliding.

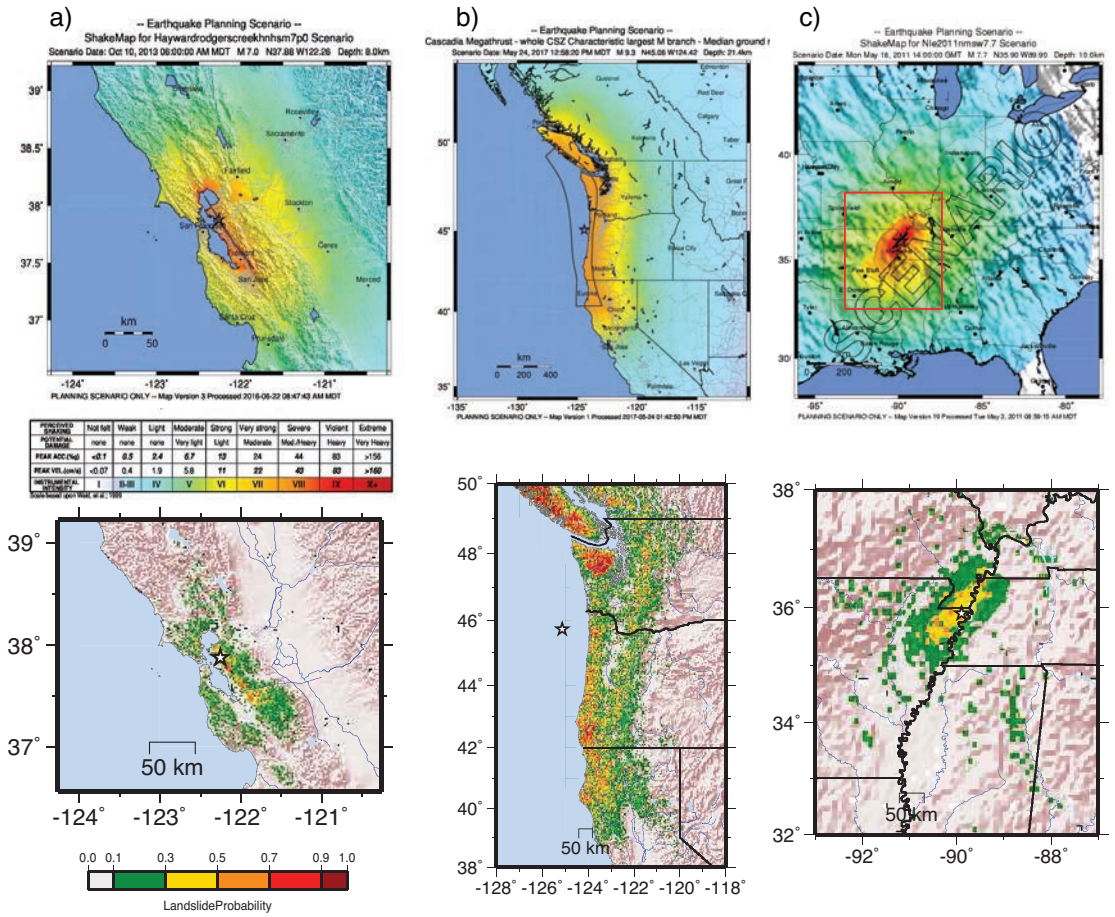

Figure 14. Top: ShakeMaps showing the spatial distribution of ground shaking for three scenario earthquakes. Bottom: Landslide probability maps. a) M7.0 Hayward fault scenario; b) M9.3 Cascadia megathrust scenario; c) M7.7 New Madrid scenario (red box indicates the map area shown by the probability map).

Application of Landslide Model to Costa Rica

Costa Rica offers a rich variety of seismotectonic source areas, a long record of earthquake-induced landslides (EQIL) dating back to 1772, and a history of devastating landslide impacts,

allowing us to test the applicability of our global near-real-time landslide model in a regional context. Through a new collaboration with the University of Costa Rica and Rutgers University, we gained access to multiple mapped landslide inventories that enabled us to validate our global landslide model results with local observational data, including inventories of landslides triggered by the 2009 Cinchona Mw 6.1 (*Ruiz et al., 2019*) and Limon Mw 7.6 (*Hernandez et al., 1992*) earthquakes, as shown in Figure 15.

Following the Cinchona earthquake, a total of 4,846 coseismic landslides were mapped over an area of 519 km² using a combination of airborne light detection and ranging (LiDAR), orthophoto data, and field observations. The earthquake resulted from a 72 km² rupture of the strike-slip Ángel fault on the eastern flank of Poás Volcano, an active volcano located within the Central Volcanic Range of Costa Rica, approximately 40 km northwest of the capital city San José, and was responsible for 30 fatalities directly attributed to landsliding (*Ruiz et al., 2019*). We observe the predicted landslide probability distribution to match observed landslide occurrence well in the areas adjacent to the epicenter (Figure 16). Nearly all mapped landslides are found in areas of high predicted landslide probability, above ~0.3 probability, excluding a small area directly west of the epicenter where rough volcanic topography inhibited aerial landslide observations. We note a few small areas of predicted high probability (e.g., red patches west of -84.7° W) where landslides were not observed. However, few other areas of high landslide probability were landslide-free, and the majority of observed landslides were in relatively high-probability zones.

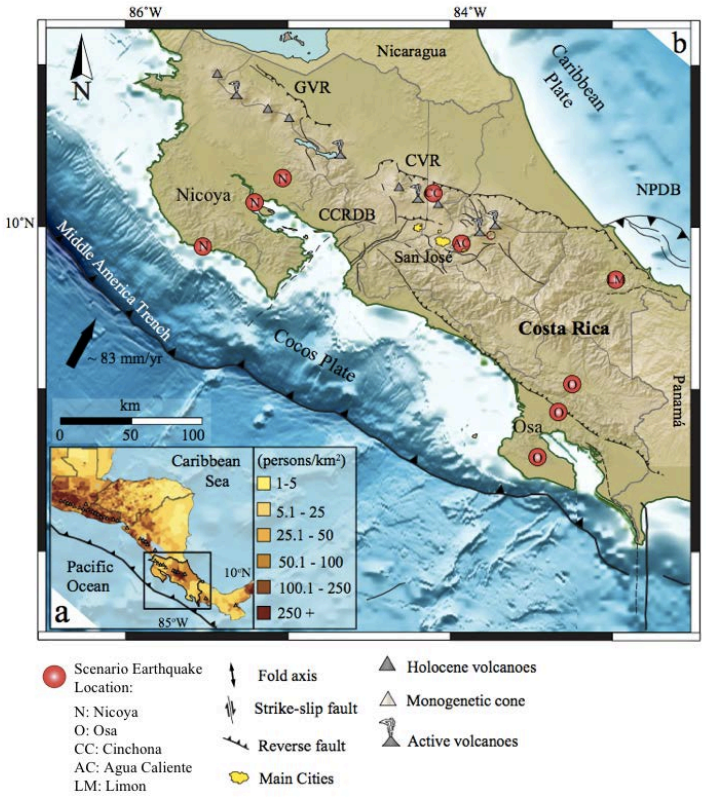

Figure 25: A.) Population distribution for the Central American Volcanic arc (CIESIN, 2005). B.) Tectonic and digital elevation map of Costa Rica, including each scenario earthquake location investigated in this study, along with the locations of major faults, population centers, and volcanoes.

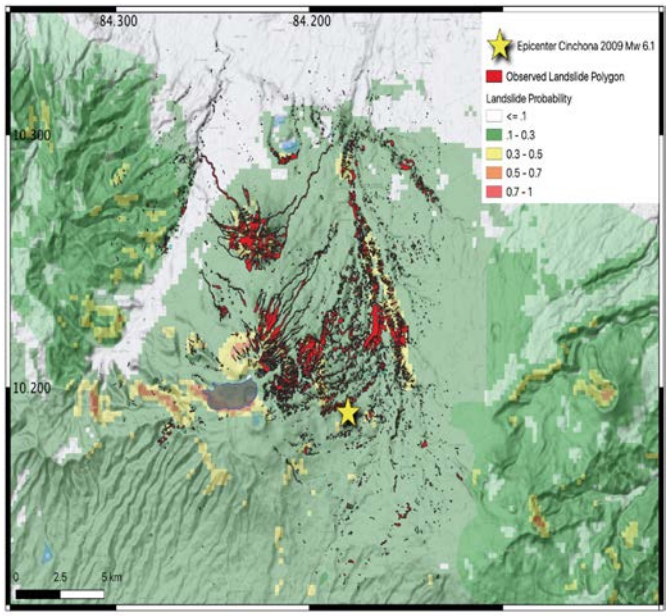

Figure 16: Comparison of predicted landslide probabilities for the 2009 Cinchona Mw 6.1 with observed mapped landslide inventories (Ruiz et al., 2019). Observed landslide polygons are drawn in red, the earthquake epicenter is denoted as a yellow star, and an area where aerial landslide mapping was inhibited by cloud cover is outlined in blue, to the west of the epicenter.

Deterministic Prediction of Landslides and Impacts using Scenario Earthquakes

In order to fully encompass the full range of ground shaking and EQIL impacts possible for Costa Rica, we use the U.S. Geological Survey *ShakeMap* software (*Worden and Wald, 2016*) to compute spatial estimates of ground shaking for

both observed and anticipated future scenario earthquake events. Scenario earthquakes are a powerful approach to deterministic seismic modeling as they allow for in-depth hazard assessment in areas of interest with limited records of historical seismicity or lacking in high-quality data. We compute suites of scenario earthquakes at a range of plausible locations, magnitudes, and depths in four distinct tectonic environments in Costa Rica, as shown in Figure 15.

These include subduction megathrust events along the Cocos-Caribbean plate boundary beneath (1) the northern Nicoya peninsula and (2) the southern Osa peninsula, (3) intraplate events beneath the Central Volcanic Range (CVR), and (4) back-arc thrust events on the eastern Caribbean coast of Costa Rica. In the CVR of Costa Rica, where numerous densely populated cities are located, we compute a suite of scenario earthquakes along the Agua Caliente Fault, directly south of San Jose at the epicenter of the devastating 1910 Cartago Ms 6.4 earthquake (*Alonso-Henar et al., 2013*). Example ground shaking and landslide probability maps for a scenario M 6.1 earthquake at 5 km depth on the Agua Caliente fault are provided in Figure 17, and the relative influence of magnitude and depth on the predicted landslide probability distribution is detailed in Figure 18. We observe increasing magnitude to raise the maximum probability and total sum areal coverage, while increasing depth decreases maximum probability while increasing sum areal coverage.

Scenario Impacts

To assess potential impacts to population for each scenario, we use high-resolution *Landscan* population data (*Bright et al., 2014*) alongside predicted landslide probability to compute the probabilistic landslide exposure index (PLEI) detailed in *Nowicki Jessee et al. (2020a)* using Eq. (1), where Po is the population count per grid cell and P_L is the landslide probability per grid cell.

$$PLEI = Po \times P_L \quad (1)$$

PLEI is computed for all scenario earthquakes in each tectonic environment of Costa Rica and compared to magnitude, depth, and sum areal coverage. We find unsurprisingly that the highest potential for landslide exposure exists in the Central Volcanic Range, due to the combination of frequent earthquake activity, rugged topography, and high population density. Additionally, due to

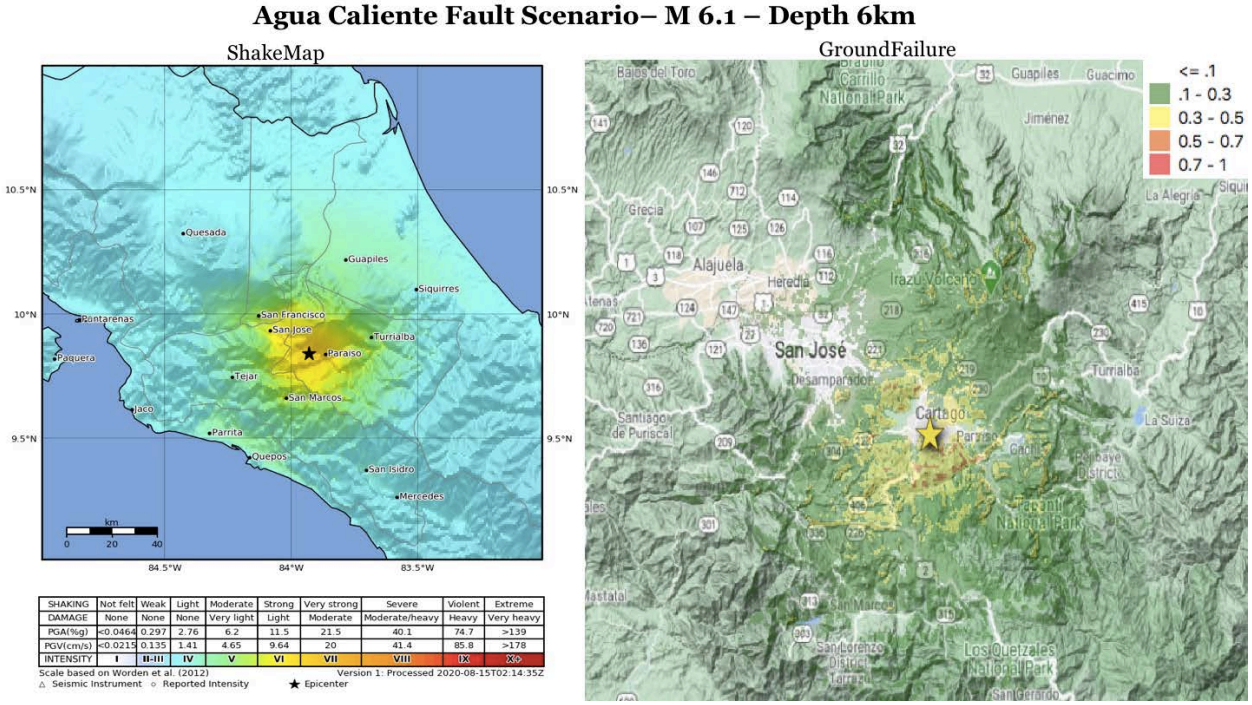

Figure 17: ShakeMap estimated ground shaking (left) and predicted GroundFailure landslide probability (right) maps for a M 6.1 scenario on the Agua Caliente Fault of Costa Rica at 6 km depth.

the potential for a large M 7.0 earthquake beneath the northern (Nicoya) and southern (Osa) portions of the Cocos-Caribbean subduction zone and related back-arc thrust events on the eastern Caribbean coast, we find that significant amounts of landslide hazard throughout the country may result from these events as well, increasing as events move inland towards central Costa Rica.

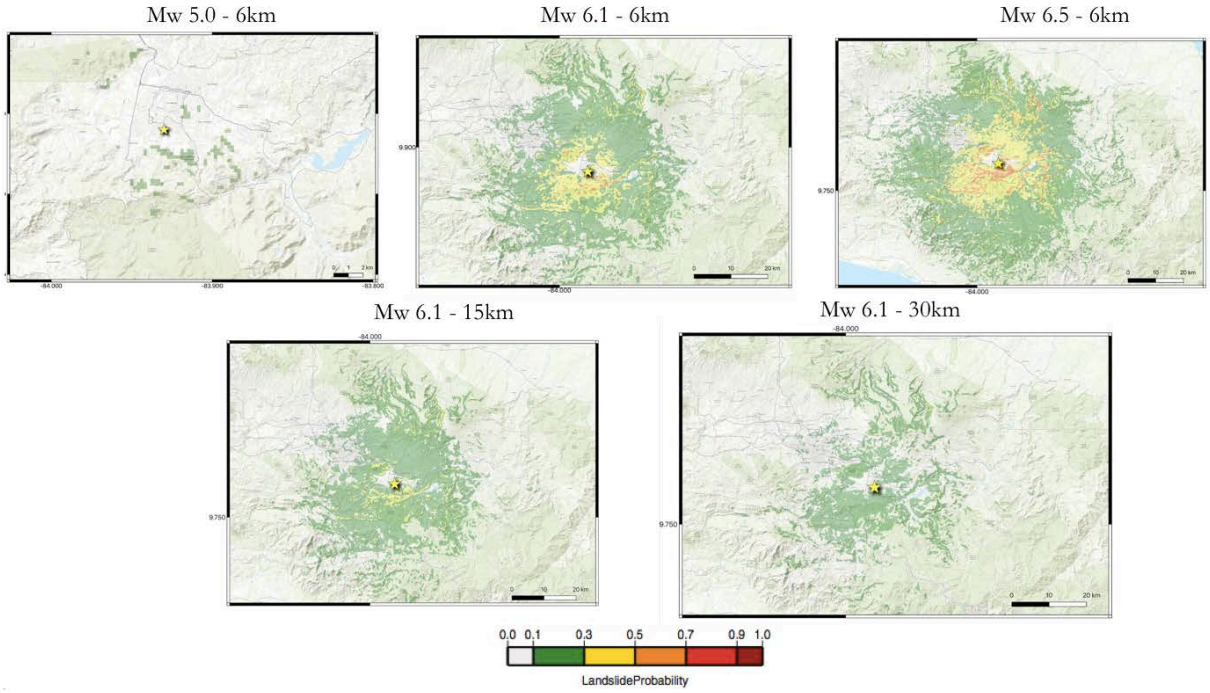

Figure 18: Distribution of predicted landslide probability for a suite of scenario earthquakes on the Agua Caliente Fault, demonstrating the impact of magnitude and depth on the spatial distribution of landslide probabilities.

Application to the Central United States

Moderate-sized crustal earthquakes originating close to populated areas can have grave impacts on the built environment in the mid-continental United States. The most seismically active zone in the central US is the New Madrid seismic zone, where three large (M > 7) earthquakes occurred in the winter of 1811-1812 (*Johnston & Schweig, 1996; Bakun & Hopper, 2004*), associated with continued activity (*Street et al., 1986*). Additional zones of seismicity include the Wabash Valley seismic zone, along the southern Illinois and Indiana border and the Anna seismic zone, located along the northern Ohio and Indiana border (*Braile et al., 1982, 1997; Bear et al., 1997; Blakely & Varma, 1976*). There have been numerous moderate-sized earthquakes in the Wabash Valley seismic zone, including the 1968 M5.5 Carbondale, Illinois earthquake and the April 2008 M5.2 Mt. Carmel, Illinois earthquake. There is growing evidence of prehistoric earthquakes in both the New Madrid and Wabash Valley seismic zones (*Tuttle et al., 2002; Obermeier et al., 1992*). The Anna seismic zone produces continued moderate-sized earthquakes, including two ~M5 earthquakes in 1937 (*Schwartz & Christensen, 1988*). While large earthquakes have been documented in this intraplate area in the historic and paleoseismic record, they occur too infrequently to provide reliable observations of earthquake-related impacts.

As a contribution to Indiana's 2019 Multi-Hazard Mitigation Plan report (*Indiana Department of Homeland Security, 2019*), we applied a deterministic seismic hazard approach to illustrate the impacts of a series of specific possible future events that might affect residents in the central United States,

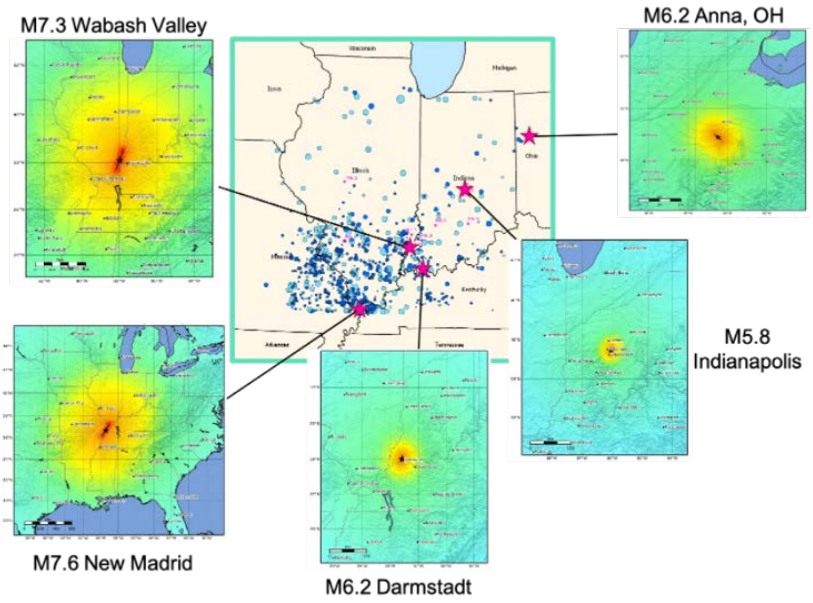

Figure 19. Locations and estimated shaking distribution for five scenario earthquakdes used in this study. Center map shows historical earthquakes as blue dots. The stars represent the approximate locations of the five scenario epicenters. Intensity maps for the five scenarios encircle the center map. Red is high intensity and blue is low intensity. Fault rupture is shown as a solid black line and the epicenter is marked with a black star.

focusing on the state of Indiana. Deterministic case studies are by definition arbitrary scenarios representing individual cases of a virtually infinite set of possible combinations of earthquake location, magnitude, source type, depth, and wave propagation characteristics that might influence the impact of earthquakes. We examined five deterministic scenarios (Figure 19) that could affect residents of the central United States; a M7.6 New Madrid event in southeastern Missouri; a M7.3 Wabash Valley event in southern Illinois; a M6.2 Anna, OH event in west-central Ohio; a M6.2 Darmstadt, IN event near Evansville; and a M5.8 Central Indiana event near Indianapolis. The locations and magnitudes were based on known fault locations and credible interpretations of the earthquake history in the region.

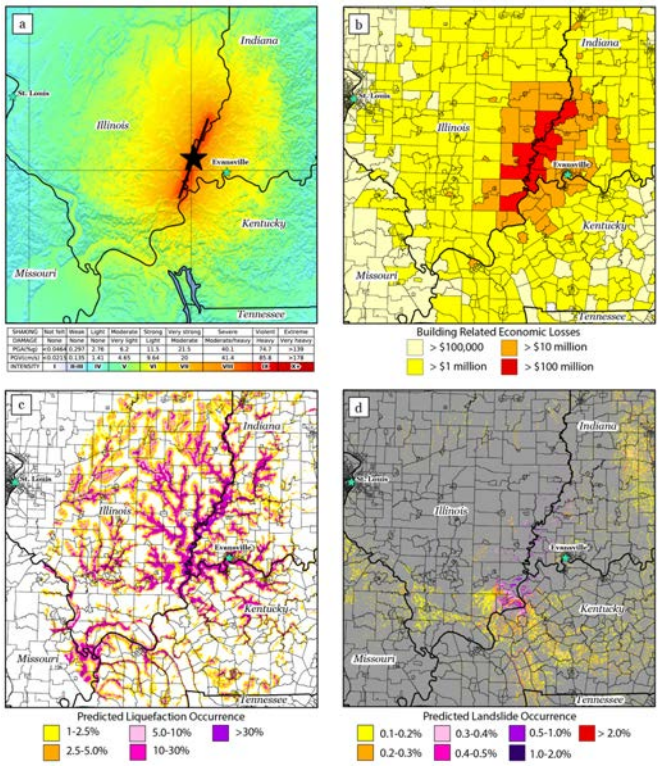

We used a combination of the US Geological Survey (USGS) *ShakeMap* and Federal Emergency Management Agency (FEMA) *Hazus-MH* software packages to assess earthquake-triggered ground-shaking and their effects on the built environment, respectively (*USGS, 2017; FEMA, 2019*). For each scenario we used *ShakeMap* to determine the spatial distribution of ground shaking and intensity, as shown for the M7.3 Wabash Valley scenario (Figure 20a). *ShakeMap* uses the location, magnitude, and source model for each event, together with geographically specific ground motion models to

Figure 20. Four maps for the M7.3 Wabash Valley scenario. (a) Shaking intensity as calculated by Shakemap. (b) HAZUS result showing monetary cost of building damage caused by scenario event. (c) Potential liquefaction occurrence as determined by the USGS Ground failure tool. (d) Potential landslide occurrence as determined by the USGS Ground failure tool.

create maps of ground motion and shaking intensity for real and scenario earthquakes. The ground shaking estimates were then used as input into *Hazus-MH* and the spatial distribution of statewide and regional building damage is mapped (Figure 20b). *Hazus-MH* is a very complex tool that can both estimate the hazard and the impact on humans and infrastructure, in principle including human casualties, economic damage, infrastructure impacts and some secondary effects. The *ShakeMap* output files were also used as inputs to our ground failure estimation tool (*Nowicki Jessee et al., 2018*) together with the *Zhu et al. (2017*) liquefaction model to examine the spatial distribution of anticipated earthquake-induced landslide and liquefaction probabilities (Figure 20c,d). The modeled landslide probabilities suggest extensive zones of moderate landslide hazard, associated with zones of higher relief in southern Illinois, central Indiana, and western Kentucky. The widespread zones of predicted liquefaction are largely controlled by proximity to unconsolidated river sediments along the Wabash and Ohio rivers, and their tributaries. This could have significant impacts on the urban areas of Evansville and Vincennes, Indiana.

Our results indicate that Indiana's built environment is significantly vulnerable to both large regional events and moderate-sized urban earthquakes, which could lead to hundreds of casualties and tens of billions of dollars in economic losses. For example, a moderate-sized earthquake located near a population center like Indianapolis or Evansville could result in economic losses greater than or equal to those due to a larger New Madrid or Wabash Valley seismic zone earthquake for those cities and the state of Indiana (Table 3). Deterministic analyses of these moderate-sized earthquakes can contribute to seismic risk assessment for areas of the central U.S. affected by rare, intraplate events. Lastly, to gain better understanding on which parameters have the greatest influence on impacts, we conducted a sensitivity analysis for earthquakes near Indianapolis and Evansville, where we reviewed losses due to differences in magnitude, depth, strike, and dip. We found that magnitude and depth have first-order influence on losses and the orientation of the causative fault in relation to populated areas can increase economic losses for an event of the same magnitude by 13-32%.

Table 3: Total economic losses for the five deterministic scenarios calculated for five regions.

Loss Calculation Area	**M7.6 New Madrid Scenario**	**M7.3 Wabash Valley Scenario**	**M6.2 Darmstadt, IN Scenario**	**M5.8 Indianapolis, IN Scenario**	**M6.2 Anna, OH Scenario**
>=10% g PGA region	$37.25 billion	$21.21 billion	$6.85 billion	$7.21 billion	$4.44 billion
State of Indiana	$839 million	$8.17 billion	$5.97 billion	$7.21 billion	$133 million
Evansville, IN	$256 million	$1.21 billion	$4.11 billion	$0	$0
Indianapolis, IN	$50 million	$421 million	$590,000	$7.15 billion	$11.7 million
Fort Wayne, IN	$150,000	$3.43 million	$0	$50,000	$133 million

This material is based upon work supported by the U.S. Geological Survey under Grant No. G19AP00027. The views and conclusions contained in this document are those of the authors and should not be interpreted as representing the opinions or policies of the U.S. Geological Survey. Mention of trade names or commercial products does not constitute their endorsement by the U.S. Geological Survey.

References

Allstadt, K. E., Jibson, R. W., Thompson, E. M., Massey, C. I., Wald, D. J., Godt, J. W., & Rengers, F. K. (2018). Improving Near-Real-Time Coseismic Landslide Models: Lessons Learned from the 2016 Kaikoura, New Zealand, Earthquake. *Bulletin of the Seismological Society of America*. https://doi.org/10.1785/0120170297

Allstadt, K. E., Thompson, E. M., Hearne, M., Wald, D. J., Nowicki Jessee, M. A., Biegel, K. M., & Hamburger, M. W. (2018). Near-Real-Time Ground Failure Estimates: A New USGS Real-Time Earthquake Product. In *ShakeMap-Related Research, Development, Operations and Applications*. Miami, FL.

Alonso - Henar, J., Montero, W., Martínez - Díaz, JJ, Álvarez - Gómez, JA, Insua - Arévalo, JM, & Rojas, W. (2013). The Aguacaliente Fault, source of the Cartago 1910 destructive earthquake (Costa Rica). *Terra Nova* , *25* (5), 368-373.

Arino, O., Perez, R., Julio, J., Kalogirou, V., Bontemps, S., Defourny, P., & Van Bogaert, E. (2012). Global Land Cover Map for 2009 (GlobCover 2009). https://doi.org/European Space Agency (ESA) & Université catholique de Louvain (UCL), doi:10.1594/PANGAEA.787668

Bakun, W. H., & Hopper, M. G. (2004). Magnitudes and locations of the 1811-1812 New Madrid, Missouri, and the 1886 Charleston, South Carolina, earthquakes. *Bulletin of the Seismological Society of America, 94*(1), 64-75.

Bear, G.W., Rupp, J. A. and Rudman, A. J. (1997). Seismic interpretation of the deep structure of the Wabash Valley Fault System, *Seism. Res. Let.* **68**, 624-640.

Bird, J. F., & Bommer, J. J. (2004). Earthquake losses due to ground failure. *Engineering Geology*, *75*(2), 147–179.

Blakely, R.F. and Varma, M. M. (1976). The seismicity of Indiana described by return periods of earthquake intensities, *Indiana Geological Survey Occasional Paper* **16**, 13 pp.

Braile, L. W., Hinze, W. J., Sexton, J. L., Keller, R. G., and Lidiak, E. G. (1982). The northeastern extension of the New Madrid seismic zone. *U.S. Geol. Surv. Prof. Paper* **1236**, 175-184.

Braile, L. W., Hinze, W. J., and Keller, G. R. (1997). New Madrid seismicity, gravity anomalies, and interpreted ancient rift structures, *Seism. Res. Let.* **68**, 599-610.

Brenning, A. (2005). Spatial prediction models for landslide hazards: review, comparison and evaluation. Retrieved from http://hal-sde.archives-ouvertes.fr/hal-00299312/

Bright, E. A., Coleman, P. R., Rose, A. N., & Urban, M. L. (2014). LandScan. *Oak Ridge: Oak Ridge National Laboratory*.

Broxton, P. D., Zeng, X., Scheftic, W., & Troch, P. A. (2014). A MODIS-based global 1-km maximum green vegetation fraction dataset. *Journal of Applied Meteorology and Climatology*, *53*(8), 1996-2004.

Budimir, M. E. A., Atkinson, P. M., & Lewis, H. G. (2015). A systematic review of landslide probability mapping using logistic regression. *Landslides*, *12*(3), 419–436. https://doi.org/10.1007/s10346-014-0550-5

Daniell, J. E., Schaefer, A. M., & Wenzel, F. (2017). Losses Associated with Secondary Effects in Earthquakes. *Frontiers in Built Environment*, *3*. https://doi.org/10.3389/fbuil.2017.00030

Federal Emergency Management Agency (2019). *Hazus-MH* (4.2). https://www.fema.gov/hazus-software

Felicísimo, Á. M., Cuartero, A., Remondo, J., & Quirós, E. (2012). Mapping landslide susceptibility with logistic regression, multiple adaptive regression splines, classification and regression trees, and maximum entropy methods: a comparative study. *Landslides*. https://doi.org/10.1007/s10346-012-0320-1

Fick, S. E., & Hijmans, R. J. (2017). WorldClim 2: new 1-km spatial resolution climate surfaces for global land areas. *International journal of climatology*, *37*(12), 4302-4315.

Gallen, S. F., Clark, M. K., Godt, J. W., Roback, K., & Niemi, N. A. (2017). Application and evaluation of a rapid response earthquake-triggered landslide model to the 25 April 2015 M w 7.8 Gorkha earthquake, Nepal. *Tectonophysics*, *714–715*, 173–187. https://doi.org/10.1016/j.tecto.2016.10.031

Garcia, D., Mah, R. T., Johnson, K. L., Hearne, M. G., Marano, K. D., Lin, K. W., et al. (2012). ShakeMap Atlas 2.0: An Improved Suite of Recent Historical Earthquake ShakeMaps for Global Hazard Analyses and Loss Model Calibration. Presented at the World Conference on Earthquake Engineering, Lisbon, Portugal.

García-Rodríguez, M. J., Malpica, J. A., Benito, B., & Díaz, M. (2008). Susceptibility assessment of earthquake-triggered landslides in El Salvador using logistic regression. *Geomorphology*, *95*(3), 172–191.

Godt, J., Sener, B., Verdin, K., Wald, D., Earle, P., Harp, E., & Jibson, R. (2008). Rapid assessment of earthquake-induced landsliding. In *Proceedings of the First World Landslide Forum, United Nations University, Tokyo, Japan*. Retrieved from http://137.227.233.24/earthquakes/pager/prodandref/Godt_et_al_(2009)_PAGER_Landslides.pdf

Hamburger, M.W., C. Geverd, D. Wald, K. Marano, K. Johnson, D. Garcia, and K. Jaiswal, 2011, Use of Scenario Earthquakes for Understanding Seismic Hazards in the APEC Region, in *School Earthquake and Tsunami Safety in APEC Economies: Reducing Risk and Improving Preparedness*, T. Tobin & K. Yawitz, eds., pp. 114-173.

Hartmann, J., & Moosdorf, N. (2012). The new global lithological map database GLiM: A representation of rock properties at the Earth surface. *Geochemistry, Geophysics, Geosystems*, *13*(12), n/a-n/a. https://doi.org/10.1029/2012GC004370

Hengl, T., Mendes de Jesus, J., Heuvelink, G. B., Ruiperez Gonzalez, M., Kilibarda, M., Blagotić, A., ... & Kempen, B. (2017). SoilGrids250m: Global gridded soil information based on machine learning. *PLoS one*, *12*(2), e0169748.

Hernández, G., Vahrson, W. y Ruiz, A. (1992). Deslizamientos producto del terremoto (4-22-91)/Landslides produced by the 22 Apr 1991 earthquake. Mapa publicado. Escuela de Ciencias Geográficas. U niversidad Nacional de Costa Rica.

Indiana Department of Homeland Security. (2019). 2019 State of Indiana Standard Multi-Hazard Mitigation Plan. Retrieved from https://www.in.gov/dhs/files/Indiana-State-Mitigation-Plan-2019-Optimized.pdf

Jibson, R. W., Harp, E. L., & Michael, J. A. (2000). A method for producing digital probabilistic seismic landslide hazard maps. *Engineering Geology*, *58*(3), 271–289.

Jibson, R. W. (2007). Regression models for estimating coseismic landslide displacement. *Engineering Geology*, *91*(2–4), 209–218.

Johnston, A. C., & Schweig, E. S. (1996). The enigma of the New Madrid earthquakes of 1811-1812. *Annual Review of Earth and Planetary Sciences, 24*(1), 339-384.

Keefer, D. K. (2002). Investigating landslides caused by earthquakes–a historical review. *Surveys in Geophysics*, *23*(6), 473–510.

Kritikos, T., Robinson, T. R., & Davies, T. R. H. (2015). Regional coseismic landslide hazard assessment without historical landslide inventories: A new approach: Coseismic landslide hazard assessment. *Journal of Geophysical Research: Earth Surface*, *120*(4), 711–729. https://doi.org/10.1002/2014JF003224

Li, W. L., Huang, R. Q., & Xu, Q. (2012). GIS-based logistic regression for landslide susceptibility mapping of the 2008 Wenchuan earthquake region, China. *Landslides and Engineered Slopes: Protecting Society through Improved Understanding*.

Liao, H. W., & Lee, C. T. (2000, December). Landslides triggered by the Chi-Chi earthquake. In *Proceedings of the 21st Asian conference on remote sensing, Taipei* (Vol. 1, No. 2, pp. 383-388).

Marano, K. D., Wald, D. J., & Allen, T. I. (2009). Global earthquake casualties due to secondary effects: a quantitative analysis for improving rapid loss analyses. *Natural Hazards*, *52*(2), 319–328. https://doi.org/10.1007/s11069-009-9372-5

Marc, O., Hovius, N., Meunier, P., Gorum, T., & Uchida, T. (2016). A seismologically consistent expression for the total area and volume of earthquake-triggered landsliding: MODELING EARTHQUAKE-TRIGGERED LANDSLIDES. *Journal of Geophysical Research: Earth Surface*, *121*(4), 640–663. https://doi.org/10.1002/2015JF003732

Marzban, C. (2004). The ROC curve and the area under it as performance measures. *Weather and Forecasting*, *19*(6), 1106–1114.

Meunier, P., Hovius, N., & Haines, A. J. (2007). Regional patterns of earthquake-triggered landslides and their relation to ground motion. *Geophysical Research Letters*, *34*(20), 1–L20408.

Moore, I. D., R. B. Grayson, and A. R. Ladson (1991), Digital terrain modelling: a review of hydrological, geomorphological, and biological applications, *Hydrol. Process.*, *5*(1), 3–30.

Nadim, F., Kjekstad, O., Peduzzi, P., Herold, C., & Jaedicke, C. (2006). Global landslide and avalanche hotspots. *Landslides*, *3*(2), 159–173. https://doi.org/10.1007/s10346-006-0036-1

Nowicki, M. A., Wald, D. J., Hamburger, M. W., Hearne, M., & Thompson, E. M. (2014). Development of a globally applicable model for near real-time prediction of seismically induced landslides. *Engineering Geology*, *173*, 54–65. https://doi.org/10.1016/j.enggeo.2014.02.002

Nowicki Jessee, M. A., Hamburger, M. W., Allstadt, K., Wald, D. J., Robeson, S., Tanyas, H., et al. (2018). A Global Statistical Model for Near Real-Time Assessment of Seismically Induced Landslides. *Journal of Geophysical Research: Earth Surface*.

Nowicki Jessee, M.A., Hamburger, M. W., Ferrara, M. R., McLean, A., & FitzGerald, C. (2020a). A global dataset and model of earthquake-induced landslide fatalities. *Landslides*, 1-14. https://doi.org/10.1007/s10346-020-01356-z

Nowicki Jessee, M. A., Seal, D., Hamburger, M. W., Sherrill, E. M., Wald, D. J., & Allstadt, K. (2020b, December). A high-resolution globally applicable model for near-real-time estimation of earthquake-induced landslides. In *AGU Fall Meeting 2020*. AGU.

Obermeier, S. F., Munson, P. J., Munson, C. A., Martin, J. R., Frankel, A. D., Youd, T. L., & Pond, E. C. (1992). Liquefaction evidence for strong Holocene earthquake(s) in the Wabash Valley of Indiana-Illinois. *Seismological Research Letters, 63*(3), 321-335.

Parker, R. N., Rosser, N. J., & Hales, T. C. (2017). Spatial prediction of earthquake-induced landslide probability. *Natural Hazards and Earth System Sciences Discussions*, 1–29. https://doi.org/10.5194/nhess-2017-193

Pelletier, J. D., Broxton, P. D., Hazenberg, P., Zeng, X., Troch, P. A., Niu, G., ... & Gochis, D. (2016). Global 1-km gridded thickness of soil, regolith, and sedimentary deposit layers. *ORNL DAAC*.

Peng, C. Y. J., Lee, K. L., & Ingersoll, G. M. (2002). An introduction to logistic regression analysis and reporting. *The Journal of Educational Research*, *96*(1), 3–14.

Rennie, J. (2003). Logistic regression. *online] Apr*, *23*.

Robinson, T. R., Rosser, N. J., Davies, T. R. H., Wilson, T. M., & Orchiston, C. (2018). Near-Real-Time Modeling of Landslide Impacts to Inform Rapid Response: An Example from the 2016 Kaikoura, New Zealand, Earthquake. *Bulletin of the Seismological Society of America*. https://doi.org/10.1785/0120170234

Rodriguez, C. E., Bommer, J. J., & Chandler, R. J. (1999). Earthquake-induced landslides: 1980-1997. *Soil Dynamics and Earthquake Engineering*, *18*, 325–346.

Ruiz, P., Carr, M. J., Alvarado, G. E., Soto, G. J., Mana, S., Feigenson, M. D., & Sáenz, L. F. (2019). Coseismic landslide susceptibility analysis using LiDAR data PGA attenuation and GIS: The case of Poás volcano, Costa Rica, Central America. In *Poás Volcano* (pp. 79-118). Springer, Cham.

Schmitt, R.G., Tanyas, Hakan, Nowicki Jessee, M.A., Zhu, J., Biegel, K.M., Allstadt, K.E., Jibson, R.W., Thompson, E.M., van Westen, C.J., Sato, H.P., Wald, D.J., Godt, J.W., Gorum, Tolga, Xu, Chong, Rathje, E.M., Knudsen, K.L., 2017, *An Open Repository ofEarthquake-triggered Ground Failure Inventories*, U.S. Geological Survey data release collection.

Schwartz, S. Y., & Christensen, D. H. (1988). The 12 July 1986 St. Marys, Ohio earthquake and recent seismicity in the Anna, Ohio seismogenic zone. *Seismological Research Letters, 59*(2), 57-62.

Sherrill, E.M & Hamburger, M.W. (2021). Use of Scenario Earthquakes for Seismic Hazard Assessment in the Central United States (abstract). *Seismological Society of America, Annual Meeting.*

Street, R., Couch, D., & Konkler, J. (1986). The Charleston, Missouri Earthquake of October 31. *Earthquake Notes, 57*(2), 41-51.

Tanyas, H., van Westen, C. J., Allstadt, K. E., Nowicki Jessee, M. A., Gorum, T., Jibson, R. W., et al. (2017). Presentation and Analysis of a World-Wide Database of Earthquake-Induced Landslide Inventories. *Journal of Geophysical Research: Earth Surface*.

Tuttle, M. P., Schweig, E. S., Sims, J. D., Lafferty, R. H., Wolf, L. W., & Haynes, M. L. (2002). The earthquake potential of the New Madrid seismic zone. *Bulletin of the Seismological Society of America, 92*(6), 2080-2089.

United Nations Development Programme (2016) Human development report 2016: human development for everyone. *http://hdr.undp.org/sites/default/files/2016_human_development_report.pdf*. Accessed 1 Sept 2017

United States Geological Survey [USGS] (2017). ShakeMap – Earthquake Ground Motion and Shaking Intensity Maps: U.S. Geological Survey. https://doi.org/10.5066/F7W957B2.

Verdin, K. L. (2017). *Hydrologic Derivatives for Modeling and Analysis - A New Global High-Resolution Database* (Data Series No. 1053). U.S. Geological Survey.

Wagenmakers, E. J., & Farrell, S. (2004). AIC model selection using Akaike weights. *Psychonomic bulletin & review*, *11*(1), 192-196.

Worden, C. B., & Wald, D. J. (2016). ShakeMap Manual Online: technical manual, user's guide, and software guide. *U.S. Geological Survey*. https://doi.org/10.5066/F7D21VPQ

Zhu, J., Baise, L. G., & Thompson, E. M. (2017). An updated geospatial liquefaction model for global application. *Bulletin of the Seismological Society of America, 107*(3), 1365-1385.

Bibliography of Work Supported by this project

Nowicki Jessee, M. A., Seal, D., Hamburger, M. W., Sherrill, E. M., Wald, D. J., & Allstadt, K. (2020, December). A high-resolution globally applicable model for near-real-time estimation of earthquake-induced landslides. In *AGU Fall Meeting 2020*. AGU.

Seal, D., Nowicki Jessee, M. A., Hamburger, M. W., & Ruiz, P. (2020, December). Application of Scenario Earthquakes for Assessment of Coseismic Landslide Hazard: A Case Study in Costa Rica. In *AGU Fall Meeting 2020*. AGU.

Ruiz, P., Rodriguez, N., Valverde, J., Marden, A., Vecchiarelli, L., Seal, D., Nowicki Jessee, M.A. and Hamburger, M.W. (2020, December). A comprehensive catalog of coseismic landslides in Costa Rica: Toward the development of an empirical landslide hazard model. In *AGU Fall Meeting 2020*. AGU.

Seal, D.M., Jessee, A.N., Hamburger, M.W., and Allstadt, K.E., 2020, Comprehensive Global Database of Earthquake-Induced Landslide Events and Their Impacts: U.S. Geological Survey data release, https://doi.org/10.5066/P9NWIRZZ.

Nowicki Jessee, M.A., E.M. Sherill, M.W. Hamburger, K.E. Allstadt, E.M. Thompson, M.G. Hearne, and D.J. Wald, 2019. Improving estimates of the likelihood of seismically induced landslides in near real-time (abstract). *American Geophysical Union Annual Meeting*, San Francisco, California.

Nowicki Jessee, M.A., M.W. Hamburger, 2019. Estimating the Likelihood and Impact of Seismically Induced Landslides in Near Real-time (abstract). *Seismological Society of America Annual Meeting*, Seattle, Washington.

Nowicki Jessee, M.A., M.W. Hamburger, M.R. Ferrara, A. McLean, C. FitzGerald, 2020, A Global Dataset and Model of Earthquake-induced Landslide Fatalities, *Landslides*.

Sherrill, E.M & Hamburger, M.W. (2021). Use of Scenario Earthquakes for Seismic Hazard Assessment in the Central United States (abstract). *Seismological Society of America, Annual Meeting.*

*Nowicki Jessee, M.A., M.W. Hamburger, K. Allstadt, D.J. Wald, S. Robeson, H. Tanyas, M. Hearne, and E.M. Thompson, 2018, A Global Empirical Model for Near Real-Time Assessment of Seismically-induced Landslides, *Journal of Geophysical Research: Earth Surface*, *123*, 1835-1859.

*Nowicki Jessee, M.A., M.W. Hamburger, K.E. Allstadt, E.M. Thompson, D.J. Wald, M.R. Ferrara, A. McLean, C. FitzGerald (May 2018). *Estimating Fatalities Associated with Seismically Induced Landslides*. Seismological Society of America Annual Meeting, Miami, Florida.

*Nowicki Jessee, M.A., M.W. Hamburger, S. Robeson, M. Ferarra and C. FitzGerald, 2017, Can We Predict the Impact of Seismically Induced Landslides? presented at 2017 Seismological Society of America Annual Meeting, Denver, Colorado, 18-20 April.

*Allstadt, K.E., E.M. Thompson, D.J. Wald, M.W. Hamburger, J.W. Godt, K.L. Knudsen, R.W. Jibson, M.A. Jessee, J. Zhu, M. Hearne, L.G. Baise, H.Tanyas, and K.D. Marano, 2016, USGS Approach to Real-Time Estimation of Earthquake-Triggered Ground Failure—Results of 2015 Workshop, *USGS Open-File Report* 2016–1044.

*Jessee, M.A. (April 2016). *Global Model for Predicting Seismically Induced Landslides in Near Real-time,* Crossroads Geology Conference, Indiana University,

*Jessee, M.A., M.W. Hamburger, D.J. Wald, M. Hearne, S. Robeson, E.M. Thompson, H. Tanyas, K. Allstadt (April 2016). *Use of an expanded global earthquake data set to develop a near real-time model for predicting seismically induced landslides.* Seismological Society of America Annual Meeting, Reno, Nevada.

*Jessee, M. Anna (October 2015). Toward a Global Model for Predicting Earthquake-Induced Landslides in Near-Real Time, USGS Geologic Hazards Science Center Secondary Hazards Workshop, Invited Talk.

*Nowicki, M.A., M.W. Hamburger, D.J. Wald, S. Robeson, M. Hearne (April 2015). *Global Model for Predicting Seismically Induced Landslides in Near Real-time.* Seismological Society of America Annual Meeting, Pasadena, California.

*Nowicki, M. Anna (July 17, 2014). *Toward a Global Model for Predicting Earthquake-Induced Landslides in Near-Real Time*, USGS Geologic Hazards Science Center Seminar Series, Invited Talk

*Nowicki, M. Anna, D.J. Wald, M.W. Hamburger, M.G. Hearne, E.M. Thomspson (February 2014). *Development of a Globally Applicable Model for Near Real-time Prediction of Seismically Induced Landslides,* Engineering Geology.

*Nowicki; M.A., D.J. Wald; M.W. Hamburger; M. Hearne; E. Thompson, 2013, Toward a Global Model for Predicting Earthquake-Induced Landslides in Near-Real Time, Abstract NH32A-02, presented at 2013 Fall Meeting, AGU, San Francisco, Calif., 9-13 Dec.

*Nowicki, M. Anna (June 2013). *Development of a Globally Applicable Model for Near Real-time Prediction of Seismically Induced Landslides* (Master's thesis). Indiana University, Bloomington, IN.

*Nowicki, M.A. ; M. Hearne; E. Thompson; D.J. Wald, M.W. Hamburger, 2012, Logistic Regression for Seismically Induced Landslide Predictions: Using Uniform Hazard and Geophysical Layers as Predictor Variables [abstract], *EOS, Trans. AGU, Fall Meeting, Supp.,* Abstract NH13A-1586.

**Based on work that was started before the funding period for this grant began.*